JCTC Journal of Chemical Theory and Computation

Article

pubs.acs.org/JCTC

Two-Component Relativistic Calculations of Electric-Field Gradients Using Exact Decoupling Methods: Spin−orbit and Picture-Change Effects

Jochen Autschbach,[†,*] Daoling Peng,[‡] and Markus Reiher[‡]

[†] Department of Chemistry, University at Buffalo, State University of New York, Buffalo, New York 14260-3000, United States

[‡] ETH Zürich, Laboratorium für Physikalische Chemie, Wolfgang-Pauli-Strasse 10, CH-8093 Zürich, Switzerland

ABSTRACT: Electric field gradients (EFGs) for heavy nuclei in diatomic molecules (hydrogen halides and group-13 iodides), uranyl (UO_2^{2+}), and a uranyl carbonate complex, were computed with different formally exactly (or nearly exactly) decoupled two-component relativistic Hamiltonians: the "exact two-component" (X2C) method, the Barysz−Sadlej−Snijders (BSS) approach, and up to 35th order in the Douglas−Kroll−Hess (DKH) expansion, utilizing a new implementation in the open-source NWChem quantum chemistry package. Results from two-component Hartree−Fock and density functional theory (DFT) calculations at the scalar relativistic approximation as well as including spin−orbit coupling are reported. Picture-change corrected EFGs obtained with X2C, BSS, and high-order DKH are shown to be numerically equivalent. Effects from spin−orbit coupling on the EFGs tend to be moderate but should not be excluded for reliable predictions. Picture-change effects on the EFG of a heavy atom can be as large as the correct picture-change corrected value, as is shown for the uranium EFG in the uranyl systems. The results demonstrate the necessity of simultaneously including spin−orbit and picture-change effects in calculations of heavy atom EFGs.

1. INTRODUCTION

In the framework of relativistic quantum chemistry,[1−5] theoretical methods for calculations of electric field gradients (EFGs) at the positions of atomic nuclei continue to receive considerable interest. The EFG is a molecular property that is best calculated with an all−electron basis, at least for the atom of interest. EFGs are known to be sensitive to relativistic effects.[6,7] This is not surprising given that the relevant nonrelativistic and four-component relativistic operators have an inverse cubic dependence on the distance from the nucleus of interest (expressions are provided in Section 2), and given the fact that the electron density in a heavy atom is particularly strongly modified near the nucleus by relativistic effects.

Electric field gradients at atomic nuclei are of great practical relevance in spectroscopy. The quadrupole moment of an atomic nucleus with spin greater than $^1/_2$ interacts with the EFG caused by surrounding charge distributions (nuclei and electrons). This quadrupolar interaction is directly probed in nuclear quadrupole resonance (NQR)[8,9] experiments, and it is important also for many other spectroscopic methods, for instance in nuclear magnetic resonance (NMR),[7,8] Mössbauer spectroscopy,[10,11] and other high−resolution spectroscopic techniques. Quadrupolar coupling interactions manifest themselves in solution NMR spectra as line broadening arising from transverse relaxation mechanisms[12] and may be used to derive information about the local symmetry, or lack thereof, of the quadrupolar nucleus if no other structural information is available.[7] In solid-state NMR, quadrupolar interactions strongly influence the shape of the spectrum. Therefore, much structural information can be obtained from the knowledge of the principal components and orientation of the EFG tensors, in addition to the information obtained from shielding tensors and spin−spin coupling. Consequently, a significant amount of work has been devoted to accurate calculations of EFGs with the aim of rationalizing the relationship with molecular structure and the influence from the surrounding (e.g., in the solid state).[6,7,13−15]

In four-component (4c) variational relativistic quantum chemical methods the electronic contribution to the EFG is straightforwardly calculated as an integral over the electron charge density distribution multiplied with the field-gradient operator.[16] An explicit 4c approach may be computationally too expensive for large molecules due to the need for optimizing and storing both the upper ("large") and lower ("small") components of the wave function or the orbitals. An alternative way for computing EFGs in molecules, clusters, and solids with heavy elements employs a two-component (2c) relativistic framework. Traditionally, this route has been explored in conjunction with approximate 2c one-electron Hamiltonians ("quasi-relativistic" methods), in some cases augmented with approximate relativistic corrections of the electron−electron interaction. In recent years, developments have taken place to obtain matrix representations of formally exact two-component one-electron Hamiltonians, which are based on approaches for the exact decoupling of the 4c Dirac operator, for electronic structure calculations. Among these methods are the so-called normalized elimination of the small component (NESC),[17−23] "exact two-component" (X2C)[24−33] [see ref 4 for information regarding the origin of the acronym, and ref 34 for a comment on the relationship of X2C with NESC], Barysz−Sadlej−Snijders (BSS),[35−38] and arbitrary-order Douglas−Kroll−Hess (DKH).[39−44]

Received: July 20, 2012
Published: August 13, 2012

   dx.doi.org/10.1021/ct300623j | *J. Chem. Theory Comput.* 2012, 8, 4239−4248

In the context of calculating molecular properties with two-component methods, the so-called picture-change effect,[45−48] which can be very large for EFGs in particular,[48] becomes an issue. Properties such as electronic multipole moments and EFGs can be obtained from an integration of a position-dependent operator with the electron density. In the following, the modulus square of the 2c wave function is referred to as the 2c density. This density does not represent the correct relativistic electron charge distribution. The differences between the 4c (the correct one) and the 2c density are of order c^{-2}, with c being the speed of light. Therefore, these differences are of the same leading order as other relativistic effects. Consequently, within the 2c framework the calculation of EFGs and other properties that depend on the electron charge distribution requires evaluating additional terms that account for these differences. The concept of picture-change may be understood more generally as a required transformation of all operators, including the density and position operators, that must accompany a transformation of the Hamiltonian used to achieve decoupling of the positive and negative energy solutions with independent 2c wave functions. Constructing the 2c density in the usual sense from the 2c wave function, or from the 2c Kohn−Sham orbitals in density functional theory (DFT), means that the untransformed density operator is used, which introduces a picture-change.

Instead of transforming the operator and then calculating its expectation value from the 2c density, one may also reconstruct a 4c density and calculate the expectation value with the untransformed operator. Such a method was used by van Lenthe et al.[49] and by Aquino et al.[50] in the framework of the quasi-relativistic zeroth−order regular approximation (ZORA) and density functional theory (DFT). The approach, dubbed ZORA-4, was shown to provide reasonable results for EFGs in a variety of molecules, transition metal complexes, and actinide compounds, at an affordable computational expense. A similar method has also been investigated in ref 51 using scalar DKH and ZORA Hamiltonians. A reconstruction of the 4c density can of course also be employed in exact decoupling methods; it will give the same results as the operator−transformation approach. The former tends to be more efficient in conjunction with numerical integration, while the latter tends to be more suitable for analytical techniques. Picture-change corrections in EFG calculations based on operator transformations have been studied at low and higher orders of the DKH transformation,[43,52] albeit only in a scalar relativistic framework. More recently, a comparison for molecules has been made between different scalar relativistic exactly decoupled two-component methods (high-order DKH, BSS, and X2C),[53] showing that the different methods work equally well and require comparable computational effort.

Herein we report a study of picture-change effects on EFGs with exact decoupling Hamiltonians including spin−orbit (SO) coupling, along with an application to systems other than the usual series of hydrogen halides HX (X = F, Cl, Br, I, and At). A new implementation for relativistic two-component calculations within the X2C, BSS, and arbitrary-order DKH frameworks has been carried out in the massively parallel open-source NWChem package,[54] along with an implementation of a matching module to calculate picture-change corrected EFGs. In the 2c DFT module of NWChem, SO coupling can be switched off which allows the generation of scalar relativistic results for comparison with previously published EFG data obtained with scalar exact-decoupling approaches. Calculations are reported for the EFG at X for the HX series using near-complete basis sets. Further, iodine EFGs were calculated for the series of Y−I diatomics where Y = Al, Ga, In, Tl as well as for the uranium EFG in uranyl (UO_2^{2+}) and a uranyl carbonate complex, using basis sets readily available from the Pacific Northwest National Laboratory (PNNL) basis set exchange[55,56] for the latter. Picture-change effects for the test systems with heavy elements are significant, and for EFGs at uranium they approach the total magnitude of the EFG itself. For TlI we demonstrate significant SO effects on the iodine EFG which brings the calculations in line with experiment.

The paper is organized as follows: In section 2 the formalism used for the implementation is outlined. Section 3 provides computational details and basis set information. Results are presented and discussed in section 4 in the order: HX, YI, and uranyl. Section 5 summarizes the findings.

2. FORMALISM

The formalism of relativistic exact-decoupling approaches has been discussed in detail elsewhere,[53,57] and therefore only a brief outline of the technique is provided to illustrate the implementation strategy in NWChem and the functionality for relativistic two-component EFG calculations.

The notation for matrices used here is as follows: Symbols formatted as M indicate AO matrices in the basis of a set $\{\lambda_r\}$ of spin−free basis functions ("atomic orbitals", or AOs). Formatting as $\boldsymbol{M}$ is used for 2 × 2 supermatrices in two-component spinor space. For matrix representations of four-component operators we use split notation for upper (U, large) and lower (L, or small) components explicitly where it is convenient. To keep the notation in some places more compact, a notation like $\mathbb{M}$ is used to indicate a 4 × 4 supermatrix representation of a 4c operator or transformation matrix. Hartree atomic units are used throughout.

A block-diagonal (bd) relativistic one-electron Hamiltonian is obtained from the exact decoupling transformation

$$\mathbb{H}^{\mathrm{bd}} = \begin{pmatrix} \boldsymbol{H}_{UU}^{\mathrm{bd}} & 0 \\ 0 & \boldsymbol{H}_{LL}^{\mathrm{bd}} \end{pmatrix} = \mathbb{U}^{\dagger}\mathbb{H}\mathbb{U} \tag{1}$$

In eq 1, $\mathbb{H}$ is the four-component Hamiltonian matrix. Its generalized eigenvalue equation

$$\mathbb{H}\mathbb{C} = \mathbb{S}\mathbb{C}\boldsymbol{\varepsilon} \tag{2}$$

has both positive energy solutions ($\varepsilon_i > 0$) and negative energy solutions ($\varepsilon_i < 0$). For negatively charged electrons, the latter can be discarded in electronic structure calculations. The 2c electrons-only equation

$$\boldsymbol{H}_{UU}^{\mathrm{bd}}\boldsymbol{C} = \boldsymbol{S}\boldsymbol{C}\boldsymbol{\varepsilon} \tag{3}$$

has only the desired positive energy solutions ($\varepsilon_i > 0$), and only this 2c one-electron Hamiltonian is used in the relativistic quantum chemical calculations. The exact decoupling transformation

$$\mathbb{U} = \begin{pmatrix} \boldsymbol{U}_{UU} & \boldsymbol{U}_{UL} \\ \boldsymbol{U}_{LU} & \boldsymbol{U}_{LL} \end{pmatrix} \tag{4}$$

then plays a key role in the evaluation of the 2c Hamiltonian matrix. For an electrons-only Hamiltonian, only $\boldsymbol{U}_{UU}$ and $\boldsymbol{U}_{LU}$ are required. There exist several schemes (i.e., X2C, BSS, and infinite-order DKH) to obtain the exact decoupling trans-

formation $\mathbb{U}$. In the following, we use the X2C scheme (which has the simplest formulation), to outline the procedure of evaluating the exact decoupling transformation as well as the Hamiltonian matrix.

The modified Dirac equation

$$\begin{pmatrix} \boldsymbol{V} & \boldsymbol{T} \\ \boldsymbol{T} & (\frac{1}{4c^2}\boldsymbol{W} - \boldsymbol{T}) \end{pmatrix} \begin{pmatrix} \boldsymbol{C}_U \\ \boldsymbol{C}_L \end{pmatrix} = \begin{pmatrix} \boldsymbol{S} & \boldsymbol{0} \\ \boldsymbol{0} & \frac{1}{2c^2}\boldsymbol{T} \end{pmatrix} \begin{pmatrix} \boldsymbol{C}_U \\ \boldsymbol{C}_L \end{pmatrix} \boldsymbol{\varepsilon}, \quad (5)$$

which is equivalent to the 4c Dirac equation with a restricted kinetic balance (RKB)[58−61] basis set, is the target 4c equation to be exactly decoupled by a matrix transformation. Here, $\boldsymbol{C}_U$ and $\boldsymbol{C}_L$ are the coefficient matrices of the positive energy solutions for the upper and lower components (with two spin components each), respectively, c is the speed of light, and

$$\boldsymbol{S} = \begin{pmatrix} \mathrm{S} & 0 \\ 0 & \mathrm{S} \end{pmatrix}, \quad \boldsymbol{T} = \begin{pmatrix} \mathrm{T} & 0 \\ 0 & \mathrm{T} \end{pmatrix}, \quad \boldsymbol{V} = \begin{pmatrix} \mathrm{V} & 0 \\ 0 & \mathrm{V} \end{pmatrix} \quad (6)$$

are constructed from the usual nonrelativistic overlap (S), kinetic energy (T), and one-electron potential energy (V) AO matrices. Further,

$$\boldsymbol{W} = \begin{pmatrix} \mathrm{W}^0 + i\mathrm{W}^z & \mathrm{W}^y + i\mathrm{W}^x \\ -\mathrm{W}^y + i\mathrm{W}^x & \mathrm{W}^0 - i\mathrm{W}^z \end{pmatrix} \quad (7)$$

with elements

$$W_{rs} = \langle \lambda_r | (\boldsymbol{\sigma}\cdot\hat{\mathbf{p}}) V (\boldsymbol{\sigma}\cdot\hat{\mathbf{p}}) | \lambda_s \rangle \lambda_r \quad (8)$$

Here, $\hat{\mathbf{p}} = -i\nabla$ is the linear momentum vector operator in its position representation, V is the potential, and $\boldsymbol{\sigma}$ is the 3-vector of the Pauli spin matrices. The individual real matrix elements in the object $\boldsymbol{W}$ in eq 7 read

$$W^0_{rs} = \langle \lambda_r | \hat{p}_x V \hat{p}_x + \hat{p}_y V \hat{p}_y + \hat{p}_z V \hat{p}_z | \lambda_s \rangle \quad (9a)$$

$$W^x_{rs} = \langle \lambda_r | \hat{p}_y V \hat{p}_z - \hat{p}_z V \hat{p}_y | \lambda_s \rangle \quad (9b)$$

$$W^y_{rs} = \langle \lambda_r | \hat{p}_z V \hat{p}_x - \hat{p}_x V \hat{p}_z | \lambda_s \rangle \quad (9c)$$

$$W^z_{rs} = \langle \lambda_r | \hat{p}_x V \hat{p}_y - \hat{p}_y V \hat{p}_x | \lambda_s \rangle \quad (9d)$$

To obtain the X2C one-electron operator, one first need to calculate the matrix elements for S, T, V and the elements in eqs (9) for the chosen system and basis set. The calculation proceeds with the solution of the generalized one-electron matrix eigenvalue equation 5 for positive energy states. From the solution, one obtains the matrix $\boldsymbol{X}$, which is the matrix representation of the operator that produces the lower components of the positive energy eigenfunctions of the Dirac one-electron Hamiltonian from the upper components,

$$\boldsymbol{X}\boldsymbol{C}_U = \boldsymbol{C}_L \quad (10)$$

that is, formally,

$$\boldsymbol{X} = \boldsymbol{C}_L \boldsymbol{C}_U^{-1} \quad (11)$$

The components of $\mathbb{U}$ are obtained as follows:

$$\boldsymbol{U}_{UU} = \boldsymbol{S}^{-1/2}(\boldsymbol{S}^{-1/2}\tilde{\boldsymbol{S}}\boldsymbol{S}^{-1/2})^{-1/2}\boldsymbol{S}^{1/2}; \quad \boldsymbol{U}_{LU} = \boldsymbol{X}\boldsymbol{U}_{UU} \quad (12)$$

where

$$\tilde{\boldsymbol{S}} = \boldsymbol{S} + \frac{1}{2c^2}\boldsymbol{X}^\dagger \boldsymbol{T}\boldsymbol{X} \quad (13)$$

The X2C two-component Hamiltonian represented in the RKB basis is then the upper diagonal block of the matrix $\mathbb{H}^{\mathrm{bd}}$ in eq 1

$$\boldsymbol{H}^{\mathrm{bd}}_{UU} = \boldsymbol{U}^\dagger_{UU}\boldsymbol{V}\boldsymbol{U}_{UU} + \boldsymbol{U}^\dagger_{UU}\boldsymbol{T}\boldsymbol{U}_{LU} + \boldsymbol{U}^\dagger_{LU}\boldsymbol{T}\boldsymbol{U}_{UU} + \boldsymbol{U}^\dagger_{LU}\left(\frac{1}{4c^2}\boldsymbol{W} - \boldsymbol{T}\right)\boldsymbol{U}_{LU} \quad (14)$$

The EFG is defined via the second derivative of the electric potential at a position $\mathbf{r}$ in a molecule. It has a nuclear and an electronic component

$$V^{\mathrm{nuc}}_{pq}(\mathbf{r}) = \frac{\partial^2}{\partial r_p \partial r_q}\left(\sum_A \frac{Z_A}{|\mathbf{r} - \mathbf{R}_A|}\right) = \sum_{A, \mathbf{R}_A \neq \mathbf{r}} Z_A \hat{Q}_{pq}(\mathbf{r}, \mathbf{R}_A) \quad (15a)$$

$$V^{\mathrm{el}}_{pq}(\mathbf{r}) = \frac{\partial^2}{\partial r_p \partial r_q}\left(-\int \mathrm{d}^3 r' \frac{\rho(\mathbf{r}')}{|\mathbf{r} - \mathbf{r}'|}\right) = -\int \mathrm{d}^3 r' \rho(\mathbf{r}') \hat{Q}_{pq}(\mathbf{r}, \mathbf{r}') \quad (15b)$$

where $-\rho$ is the electron charge-density, $\mathbf{R}_A$ is the position of point-nucleus A, and $p,q \in \{x,y,z\}$. In eqs (15), the point-quadrupole operator $\hat{Q}_{pq}(\mathbf{r}, \mathbf{r}')$ is given as

$$\hat{Q}_{pq}(\mathbf{r}, \mathbf{r}') = \frac{3(r_p - r_p')(r_q - r_q') - \delta_{pq}(\mathbf{r} - \mathbf{r}')^2}{|\mathbf{r} - \mathbf{r}'|^5} \quad (16)$$

Since the relevant parts of the transformation matrix $\mathbb{U}$ are constructed explicitly for exact decoupling methods, they can be used further to transform the quadrupole operator in the expression for $V^{\mathrm{el}}_{pq}(\mathbf{r})$ such that the two-component density can be used for the evaluation of EFGs. In the implementation, the following property matrix elements are calculated in the uncontracted AO basis in order to calculate the picture-change corrected EFG tensor component p,q at the position $\mathbf{R}$ of one of the nuclei. Define the operator $\hat{Q}$ as the p,q component of eq 16 for $\mathbf{r} = \mathbf{R}$, to obtain matrix elements:

$$Q^U_{rs} = \langle \lambda_r | \hat{Q} | \lambda_s \rangle \quad (17a)$$

$$Q^L_{rs} = \langle \lambda_r | (\boldsymbol{\sigma}\cdot\hat{\mathbf{p}})\, \hat{Q}\, (\boldsymbol{\sigma}\cdot\hat{\mathbf{p}}) | \lambda_s \rangle \quad (17b)$$

(the integration goes over $\mathbf{r}'$) to construct

$$\boldsymbol{Q}_{UU} = \begin{pmatrix} \mathrm{Q}^U & 0 \\ 0 & \mathrm{Q}^U \end{pmatrix}, \quad \boldsymbol{Q}_{LL} = \begin{pmatrix} \mathrm{Q}^{L,0} + i\mathrm{Q}^{L,z} & \mathrm{Q}^{L,y} + i\mathrm{Q}^{L,x} \\ -\mathrm{Q}^{L,y} + i\mathrm{Q}^{L,x} & \mathrm{Q}^{L,0} - i\mathrm{Q}^{L,z} \end{pmatrix} \quad (18)$$

where the matrix elements $Q^{L,\{0,x,y,z\}}_{rs}$ have the same structure as the matrix elements in eq 9 with V replaced by $\hat{Q}$. The two-component operator matrix is then calculated from

$$\boldsymbol{Q} = \boldsymbol{U}^\dagger_{UU}\boldsymbol{Q}_{UU}\boldsymbol{U}_{UU} + \frac{1}{4c^2}\boldsymbol{U}^\dagger_{LU}\boldsymbol{Q}_{LL}\boldsymbol{U}_{LU} \quad (19)$$

The picture-change corrected electronic EFG component p,q at nuclear position $\mathbf{R}$ is finally obtained from $\boldsymbol{Q}$ and the two-

dx.doi.org/10.1021/ct300623j | J. Chem. Theory Comput. 2012, 8, 4239−4248

component density matrix $\boldsymbol{P}$ as tr[$\boldsymbol{PQ}$], whereas the EFG component without picture-change correction is given as tr[$\boldsymbol{PQ}_{UU}$].

Other exact decoupling approaches only differ in the step of constructing the decoupling transformation matrices $\boldsymbol{U}_{UU}$ and $\boldsymbol{U}_{LU}$, and they provide different decoupling matrices than the X2C method. The subsequent procedure for the picture-change correction of property matrices is the same for all exact decoupling methods and thus they employ the same program code. One should note that all of the above matrices must be constructed using an uncontracted AO basis. A basis contraction of the Hamiltonian and property operator matrices can be performed after the relativistic transformation step (instead of entering the relativistic transformation procedure with operator matrices in a contracted AO basis representation).

3. COMPUTATIONAL DETAILS

The exact-decoupling functionality for ground-state two-component calculations, and a module for EFG calculations based thereupon, has been implemented in a developer's version of the NWChem 6 package,[62−64] as an extension of its two-component DFT module. Scalar relativistic reference data were produced with the same program module, by deleting the spin-dependent elements 9b to 9d of the $\boldsymbol{W}$ matrix before the decoupling transformation, and by deleting the corresponding spin-dependent elements in $\boldsymbol{Q}_{LL}$ in eq 17b prior to the picture-change transformation of the EFG operator matrix.

For the hydrogen halide benchmark, basis sets deemed to be close to the basis set limit have been taken from ref 43. For the group-13 iodides, the same basis sets were used as in a recent benchmark of the ZORA-4 approach:[50] for Al, Ga, In, and I, we adopted the basis sets devised by Tsuchiya-Abe-Nakajima-Hirao[65] (TANH) and augmented them with polarization functions from the TZVPP[66] triple-ζ valence polarized basis available at the PNNL basis set exchange.[55,56] For Tl, the ANO-RCC[67] basis was used, with angular momentum functions for $l > 3$ removed. We found in the previous ZORA-4 study that these basis sets represent a suitably accurate choice for DFT-based calculations of EFGs. For the uranyl systems, the ligand basis was chosen as TZVPP, while for U the ANO-RCC basis set was used, with angular momentum functions for $l > 4$ removed. All basis sets were fully uncontracted. For the present benchmark, the calculations employed nuclear point charges.

Computations were carried out at the Hartree−Fock (HF) level, and with the DFT using the following functionals: the Becke88[68] + Perdew86[69] (BP) nonhybrid functional, and the Becke88[68] + Lee−Yang−Parr[70] (LYP)[71] three-parameter hybrid[70] B3LYP.[72] Computations based on hybrid functionals with range-separated exchange can also be performed with the implementation. The performance of such functionals in exact-decoupling based EFG calculations for systems that are highly sensitive to approximations in the functional will be considered in a forthcoming paper. However, for comparison with HF, BP, and B3LYP, we report some results obtained with the CAM-B3LYP functional[73] in the present study. This functional goes to 65% HF exchange asymptotically for large interelectronic separations r_{12} and affords 19% HF exchange for $r_{12}\rightarrow 0$.

Calculations with the exact decoupling approaches have been carried out with two different potentials V used for the evaluation of the transformation matrix: In most cases the external potential V_{ext} (i.e., the electron−nucleus potential) has been used. To improve the relativistic description of effective potentials arising from electron−electron interactions, which have significant influence on the spin−orbit splittings of heavy atoms but may also influence other calculated properties, a version with a model potential[29,31,74] V_{mp} was also implemented. In this case the potential was chosen to be the external potential plus the Hartree potential of the initial atomic fragment guess used in the Hartree−Fock and DFT computations. The potential is the same that has been used previously to construct the relevant operators for ZORA-4 calculations of field gradients with NWChem[50] and to construct the Hamiltonian for the ZORA DFT code in NWChem.[54] Most of the required one-electron integrals for the evaluation of exact decoupling Hamiltonian matrices and the picture-change corrected EFG were already available analytically in NWChem, with two exceptions. To facilitate the present proof-of-concept study, the Hartree part of the model potential in the matrix elements of eqs 9, and the lower-component basis matrix Q_L of eq 17b have been obtained with numerical integration. Comparisons with a previous fully analytical scalar implementation[43] have been made to confirm that the Q_L matrix elements are accurate. We plan to implement the missing analytic integrals in the future; however, it is noted that the results reported in this work are not negatively impacted by the use of numerical integration.

4. RESULTS AND DISCUSSION

4.1. Hydrogen Halides HX, X = F, Cl, Br, I, At. An article on electric field gradients reporting tests of a new quantum chemistry method or a new implementation would not be complete without the hydrogen halide (HX, X = F, Cl, Br, I, At) benchmark. Table 1 lists EFGs at the halide nuclei for the series obtained with Hartree−Fock and DFT X2C calculations using the BP functional. The values reported in Table 1, and elsewhere in this work, represent the largest-magnitude principal component V_{33} of the traceless rank-2 tensor defined by eqs 15. For linear molecules, V_{33} is in the direction of the molecular axis.

The basis sets used for the HX benchmark are the same as used previously by some of us[43] which are thought to be close to the basis set limit. The comparison between HF and DFT with the BP functional shows that the heavy-atom EFG in the series is not particularly sensitive to correlation effects. Use of the hybrid functional (CAM-B3LYP, with range-separated exchange) is also seen to affect the results only moderately. For this reason, we decided to forego CAM-B3LYP calculations with the BSS and DKH Hamiltonians (vide infra). Along the series, the picture-change effects become comparable in magnitude to the differences between the different functionals and Hartree−Fock theory for HBr, and larger for HI and HAt. For iodine, the picture-change effects reach a magnitude of over 1 atomic unit (au), and therefore they cannot be neglected. The example of HAt shows that picture-change effects on EFGs can become dramatically large if the atom is sufficiently heavy. The calculations for uranyl complexes (vide infra) demonstrate even larger picture-change effects.

We also performed the BSS and DKH calculations for the HX series. The results of Hartree−Fock and DFT (BP functional) calculations are collected in Tables 2 and 3. The DKH calculations are reported here for the 35th order of the transformation. Test calculations for higher orders in the DKH transformation did not significantly improve the accuracy, which means that this (already high) DKH order can be considered exact for practical purposes. The BSS picture change

Table 1. Halide Field Gradient (V_{33}, in Atomic Units (au) for Hydrogen Halides[a] Scalar and Spin-Orbit (SO) X2C Calculations Using V_{ext} for the Transformation (Model Potential Where Indicated by "mp")

		pcc[b]	HF	HCl	HBr	HI	HAt
HF	scalar	–	2.814	3.619	7.821	12.748	35.282
		√	2.809	3.590	7.537	11.628	26.698
	SO	–	2.814	3.618	7.810	12.642	32.772
		√	2.809	3.590	7.534	11.609	25.995
	SO-mp	–	2.814	3.619	7.815	12.656	32.877
		√	2.810	3.591	7.538	11.622	26.077
DHF[c]			2.810	3.591	7.540	11.623	25.980
BP	scalar	–	2.717	3.529	7.725	12.296	32.284
		√	2.712	3.501	7.451	11.245	24.631
	SO	–	2.717	3.529	7.711	12.149	29.137
		√	2.712	3.501	7.444	11.191	23.390
CAM[d]	scalar	–	2.716	3.604	7.912	12.792	34.191
		√	2.711	3.576	7.628	11.688	26.009
	SO	–	2.716	3.604	7.897	12.644	30.967
		√	2.711	3.576	7.622	11.635	24.771

[a]Uncontracted basis sets and geometries from Mastalerz et al.,[43] H(20s5p4d), F(23s17p6d4f), Cl(24s19p7d5f), Br(30s22p14d8f3g), I(35s28p19d8f4g), At(37s32p22d15f4g). Internuclear distances in bohr: HF = 1.732549, HCl = 2.408502, HBr = 2.672946, HI = 3.040798, HAt = 3.250392. [b]The symbol √ indicates that picture-change corrections (pcc) are included. A dash indicates that the untransformed electronic EFG operator was used. [c]Four-component Dirac–Hartree–Fock (DHF) results taken from ref 43. [d]CAM-B3LYP hybrid functional with range-separated exchange.

Table 2. Halide Field Gradient (V_{33}, in au) for Hydrogen Halides. Scalar and Spin-Orbit (SO) BSS Calculations Using V_{ext} for the Transformation except Where Indicated by "mp"[a]

		pcc	HF	HCl	HBr	HI	HAt
HF	scalar	–	2.814	3.620	7.840	12.875	37.206
		√	2.809	3.590	7.537	11.627	26.690
	SO	–	2.814	3.619	7.829	12.751	33.944
		√	2.809	3.590	7.534	11.608	25.988
	SO-mp	–	2.814	3.620	7.834	12.765	34.055
		√	2.810	3.591	7.538	11.621	26.072
BP	scalar	–	2.717	3.530	7.745	12.418	34.041
		√	2.712	3.501	7.450	11.244	24.625
	SO	–	2.717	3.530	7.730	12.252	30.163
		√	2.712	3.501	7.444	11.190	23.385

[a]See footnotes of Table 1 for further details.

corrected EFGs agree with DKH within 0.001 au. The discrepancies between BSS and X2C are also below 0.001 au except for HAt, for which they approach 0.01 au since the relativistic effects increase strongly with higher atomic number, and this also holds true for the small numerical differences among the decoupling methods. The discrepancies between EFGs calculated without picture change correction are much larger. For HAt, the differences between X2C and BSS or DKH even exceed 1 au. This indicates that the untransformed EFG results are unreliable, since different exact decoupling methods should in principle yield the same results. This is indeed the case for the picture change corrected EFGs, which is coincident with that we reported in ref 53 based on scalar relativistic molecular calculations. Therefore, it is imperative to apply the picture change correction to obtain reliable EFGs.

Table 3. Halide Field Gradient (V_{33}, in au) for Hydrogen Halides. Scalar and Spin-Orbit (SO) DKH35 Calculations Using V_{ext} for the Transformation[a]

		pcc	HF	HCl	HBr	HI	HAt
HF	scalar	–	2.814	3.619	7.840	12.875	37.196
		√	2.809	3.590	7.537	11.627	26.690
	SO	–	2.814	3.618	7.829	12.747	33.833
		√	2.809	3.590	7.534	11.608	25.988
	SO-mp	–	2.814	3.621	7.834	12.762	33.943
		√	2.810	3.591	7.538	11.621	26.072
BP	scalar	–	2.717	3.529	7.745	12.418	34.032
		√	2.712	3.501	7.450	11.244	24.625
	SO	–	2.717	3.529	7.729	12.249	30.066
		√	2.712	3.501	7.444	11.190	23.385

[a]See footnotes of Table 1 for further details.

Four-component Dirac–Hartree–Fock (DHF) EFGs taken from ref 43 are also presented in Table 1 for comparison. The same basis sets (with RKB condition for the lower components) as the 2c calculations were employed, and therefore the data can be compared directly with the 2c Hartree–Fock results. For HF and HCl, the differences between 2c and 4c results are negligible within the given precision. For HBr and HI, the 4c results are closer to the scalar 2c results rather than SO if V_{ext} is used in the transformation, while for HAt the DHF EFG is close to the result of the 2c calculation with SO. If the model potential (mp) is used in the transformation instead of V_{ext}, the SO-mp EFGs are overall in very good agreement with DHF. For for HAt there remains a 0.1 au difference (0.4% of the picture-change corrected value) between DHF and the SO-mp calculation. We plan to implement a more refined relativistic model potential approach in the future,[74] which should bring the HAt EFG fully in line with the DHF reference value. In any case, the data provided in Tables 1 and 2 show that the model potential approach usually improves upon the results obtained with V_{ext} for the transformation, and most of the calculated field gradients are already very close to the 4c benchmark.

The SO effects on the EFG are seen to be small to moderate, and less important than the picture-change corrections, for the whole series. Taking HAt as an example, with the BP functional and V_{ext} for the transformation, the SO effect on the At EFG is −3 au without picture-change corrections and a bit over −1 au when picture-change effects are included. The picture-change corrections themselves exceed −7 au for scalar X2C and reach almost −6 au for the SO calculation. Previous ZORA-4 calculations (also with NWChem but utilizing smaller basis sets) with the BP functional gave a picture-change corrected ZORA-4 SO EFG of 23.441 au which agrees quite well with the corresponding X2C result of Table 1. However, the corresponding scalar ZORA-4 EFG was smaller in magnitude by 1 au. The ZORA-4 picture-change corrections were about −3 au both for scalar and SO calculations. Clearly, in the X2C calculations there is a significant impact on the SO effect depending on whether picture-change corrections are used or not. ZORA-4 is obviously a more approximate way of treating the picture-change. Results for the group-13 iodide series

discussed in the following section demonstrate that for TlI, where SO effects on the EFG are really important, the X2C calculations produce the correct (and expected) change in the iodine EFG when going from scalar to SO calculations. Further, as mentioned above the SO Hartree–Fock results in Tables 1–3 are in good agreement with four-component reference data.

4.2. Group-13 Iodides YI, Y = Al, Ga, In, Tl. Table 4 collects the results of X2C EFG calculations for group-13 iodide diatomics, along with experimental data.

Table 4. Iodine Field Gradient (V_{33}, in au) for Group-13 Iodides. Scalar (sc) and Spin-Orbit (SO) X2C Calculations with V_{ext} and V_{mp}[a]

		calcd V_{33}, with pcc				
	expt V_{33}[b]	sc, V_{ext}	SO, V_{ext}	sc, V_{mp}	SO, V_{mp}	SO-Z4[c]
AlI	1.88(3)	1.823	1.814	1.825	1.817	1.830
GaI	2.26(4)	2.172	2.166	2.174	2.168	2.193
InI	2.36(4)	2.292	2.325	2.294	2.324	2.339
TlI	2.68(5)	2.339	2.787	2.341	2.762	2.539
		calcd V_{33}, no pcc				
	expt. V_{33}	sc, V_{ext}	SO, V_{ext}	sc, V_{mp}	SO, V_{mp}	
AlI	1.88(3)	1.978	1.963	1.980	1.966	
GaI	2.26(4)	2.364	2.345	2.366	2.348	
InI	2.36(4)	2.496	2.510	2.498	2.509	
TlI	2.68(5)	2.549	2.983	2.551	2.957	

[a]B3LYP functional. Uncontracted TANH basis (ANO for Tl), polarization functions from from TZVPP. V_{ext} and V_{mp} refers to the potentials used for the X2C transformation. See section 3 for details. pcc = picture-change corrections. Internuclear distances (in Å) taken from reference 75: AlI = 2.53710, GaI = 2.57467, InI = 2.75365, TlI = 2.81367. [b]Experimental data converted from nuclear quadrupole coupling constants taken from ref 49 (originally from ref 76), using a ^{127}I quadrupole moment of 696 mbarn.[77,78] The uncertainty of the expt quadrupole moment is 12 mbarn, which was used to estimate the uncertainties of the expt V_{33} [c]Results from spin–orbit ZORA-4 calculations, using the same basis sets as the present work, ref 50.

Good performance of nonhybrid DFT and DFT with standard hybrid functionals for main group atom EFGs has been noted before.[79] Previous ZORA-4 EFG calculations[50] for a large set of iodine and chlorine EFGs in diatomic molecules have indicated a slightly better performance of the B3LYP hybrid and two parametrizations of a hybrid functional with range-separated exchange, compared to the non–hybrid functionals BP and BLYP. For indium EFGs in indium halide diatomics the calculated ZORA-4 EFGs were closest to experiment with the BP and the B3LYP functionals. Given these previous benchmark results we decided to perform the X2C calculations for the group-13 iodides with the B3LYP hybrid functional.

Figure 1 graphically displays a comparison of the calculated data with experiment, to illustrate the magnitude of the SO effects on the iodine EFGs (left panel) as well as the importance of the picture-change effects (right panel). Clearly, given the variations of the EFG with the choice of the density functional noted in ref 50, the SO effect on the iodine EFG is of practical relevance only for the heaviest member of the series, TlI, at least in DFT calculations with standard nonhybrid and hybrid functionals. Inclusion of SO coupling causes the whole calculated data set to agree reasonably well with experiment. The remaining deviations from experiment are tentatively attributed to approximations in the functional, basis set incompleteness, and potentially a lack of vibrational corrections.[77] The previous ZORA-4 benchmark on these systems showed variations among different functionals that were of comparable magnitude as the deviations between the present X2C calculations and experiment. Table 4 includes SO-ZORA-4 B3LYP data for comparison. For AlI, GaI, and InI, the agreement with the X2C results is very close. For TlI, the ZORA-4 calculation appears to fall somewhat short.

For the systems with lighter group-13 elements, the EFGs calculated without picture-change corrections agree slightly better with experiment—obviously for the wrong reasons. For TlI, where SO effects and picture-change are both important and lead to partial cancellation, the picture-change corrected results agree significantly better with experiment. The picture-change effects are seen to vary only modestly among the set of group-13 iodides, increasing in magnitude from −0.16 (scalar) and −0.15 (SO) in AlI to −0.21 and −0.20 for the TlI scalar and SO calculations, respectively. That is, the lower-component density responsible for the picture-change is mostly affecting the iodine EFG near the iodine nucleus and yields, to some degree of approximation, a local atomic correction. At the neighboring group-13 atom, the lower-component density modifies the charge density in that atom's core. Regarding the EFG at iodine, the main function both of the 2c and the 4c core density at the neighboring atom is a screening of the nuclear charge. Density differences deep in the neighboring atom's core

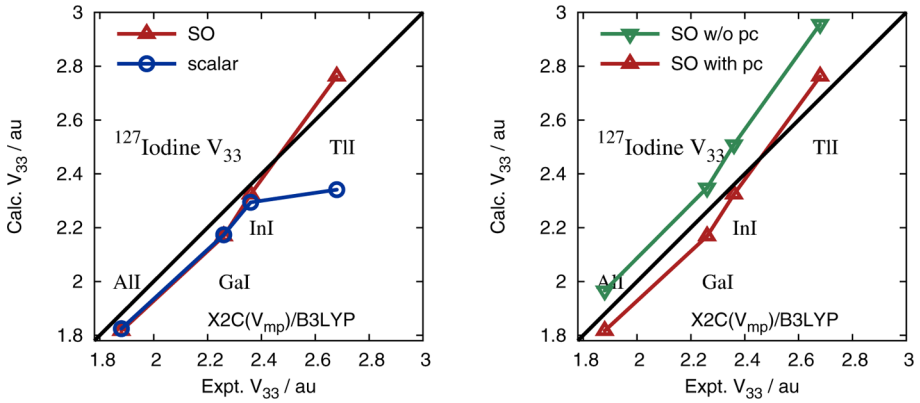

Figure 1. Iodine EFG (V_{33}, in au) in group-13 iodide diatomics. (Left) Scalar versus spin–orbit calculations. (Right) Spin–orbit calculations with and without picture-change (pc) effects. X2C with V_{mp}, B3LYP. Uncontracted TANH basis (ANO for Tl), polarization functions from from TZVPP.

are not expected to affect this screening in a significant manner. The fact that the picture-change effects do increase slightly from AlI to TlI, however, shows that the correction is not purely atomic.

For TlI, where SO effects are of the same order of magnitude as the picture-change effects, the data indicates approximate additivity of these corrections; that is, the SO effect in a calculation with and without picture-change correction is very similar, and likewise the picture-change effect is to a good approximation the same in the scalar and SO calculations. The data for the heaviest members of the HX series in section 4.1 and the uranyl data in section 4.3 show that this is not generally the case.

4.3. Uranium Field Gradients in Uranyl and Uranyl Tris-carbonate. Complexes with elements as heavy as uranium and other actinides remain a challenge for quantum chemical methods because of the simultaneous need for a description of electron−electron correlation, large basis sets, and an accurate treatment of relativistic effects.[81−83] Uranyl ions (UO_2^{2+}) are particularly important and well-studied benchmark systems for actinide electronic structure calculations (as well as for experimental methods), not the least because of their closed shell nature and chemical stability. A broader interest in studying uranium and other actinide compounds arises from the nuclear waste problem. Carbonate complexes of actinyl species are implicated in the way how actinides from nuclear waste enter the environment, since they readily form at the pH and carbonate concentrations found in natural waters.[84]

In the context of this work, the EFG at uranium is interesting for several reasons. For one, there is the sheer magnitude of picture-change effects. Further, it has been shown previously that complexation of uranyl by ligands in the equatorial plane has a profound impact on the EFG at the U center,[50,85,86] with a sign change from free UO_2 to uranyl carbonate or nitrate complexes. Experimental estimates for uranyl coordinated by three nitrate ligands, derived from Mössbauer data, place the uranium EFG in equatorially coordinated uranyl around +8 atomic units.[80] More generally, the EFG is sensitive to minor deviations of the calculated ground-state electron density from the correct density. The quality of the computational model is evidently crucial. In this context, it has been shown that EFGs at metal centers are sensitive "detectors" for deficiencies in density functionals.[50,87−90] For example, standard density functionals (in particular nonhybrid functionals) tend to overestimate the covalent character of metal−ligand bonding. If the bonding involves metal orbitals with nonzero angular momentum, the EFG at the metal center can be strongly influenced by the degree of covalency of the metal−ligand bonds. The EFGs for main-group elements, on the other hand, are known to be less sensitive to approximations in density functionals.[79]

For comparison with previous computational work,[50,85] calculations for the free uranyl ion were performed with U−O bond lengths of 1.78 Å. Figure 2 shows the geometry of the uranyl hydrogen−carbonate complex considered in this work. The geometry is based on the uranium environment found in the single-crystal X-ray diffraction (XRD) structure[82] of the uranyl salt $(NH_4)_4UO_2(CO_3)_3$. To keep the overall negative charge of the complex low, the carbonate ligands were changed to hydrogen−carbonate as detailed in ref 50.

The calculated EFGs at the uranium centers are collected in Table 5. For the X2C spin−orbit calculations with V_{mp}, Figure 2 shows graphical representations of the EFG tensors at the

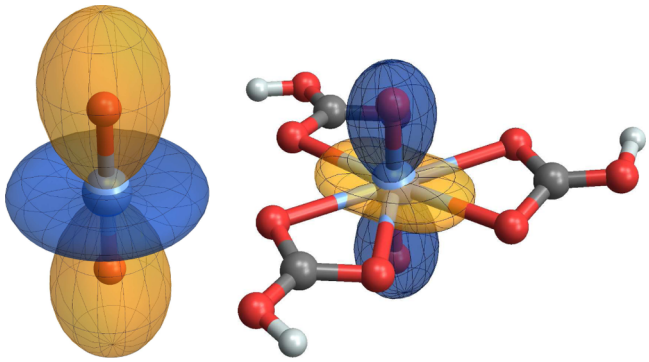

Figure 2. EFG tensors for uranyl and $[UO_2(HCO_3)_3]^-$. Polar plots of the field gradient in the direction of the field, scaled to 40 au/pm. Blue (dark shading) = positive, orange (light shading) = negative field gradient (SO X2C, V_{mp}, B3LYP).

Table 5. Electric Field Gradient (V_{33}, in au) at Uranium, in Uranyl and a Uranyl−Tris-hydrogen−carbonate Complex Used As a Model for the U Environment in $(NH_4)_4UO_2(CO_3)_3$. B3LYP Functional unless Stated Otherwise[a]

	UO_2^{2+}		$[UO_2(HCO_3)_3]^-$	
V_{33} (au)	no pcc	w/pcc	no pcc	w/pcc
SO V_{mp}	−5.558	−8.846	12.843	6.551
SO V_{ext}	−5.304	−8.697	13.222	6.807
SO V_{ext} (CAM)[b]	−3.512	−7.408	15.338	8.332
SO V_{ext} (HF)[c]	9.754	2.040	25.351	15.167
scalar V_{ext}	−4.232	−7.911	14.270	6.895

[a]Spin−orbit X2C calculations without and with (w/) picture-change corrections (pcc). Uncontracted basis sets: ANO(-h) for U, TZVPP for other atoms. Experimental estimate derived from Mössbauer data: +8.38 ± 0.13 au.[80] [b]CAM-B3LYP functional. [c]Hartree−Fock calculation.

metal center. The color coding and the extension of the polar plot surfaces indicate the sign and orientation of the principal components with respect to the molecular frame. As can be seen from the graphics, the tensor component V_{33} lies in the direction of the axis connecting the uranyl oxygens. The calculated data (DFT) and the figure demonstrate the sign change of the U EFG when going from UO_2^{2+} to the complex, that is, from negative in free uranyl to positive in the presence of equatorial ligands. This change of the uranium EFG due to equatorial coordination has been analyzed in some detail in ref 85 and ref 50. We refer the reader to ref 50 for a scalar ZORA-4 EFG analysis in terms of localized orbitals and provide only a brief summary here: Pyykkö pointed out that the positive EFG in the experimentally observed systems with equatorial coordination might be a signature of a "6p hole",[91,92] that is, a lack of electron density on the uranyl U $6p_\sigma$ orbital due to its involvement in bonding with the axial oxygens. However, the EFG in free uranyl is overall negative (with the exception of HF), in part due to a nonspherical electron distribution in the U 5*f* shell resulting from the uranyl−oxygen bonds. Only in the systems with equatorial ligands is a positive EFG computed. The donation of electronic charge from equatorial oxygen ligands into uranium $5f_\phi$ orbitals (symmetry classification with respect to free uranyl) was found to contribute about +2.5 au. The remainder of the positive change is due to relaxation of the

dx.doi.org/10.1021/ct300623j | J. Chem. Theory Comput. 2012, 8, 4239−4248

electron density around U upon equatorial coordination, which affects the bonds between U and the axial oxygens and strengthens the $6p_\sigma$-hole effect significantly.

The comparison of the calculated EFGs in Table 5 demonstrates that picture-change effects are essential for predictions of uranium EFGs by two-component relativistic methods. The nuclear contributions to the EFG at the U center are very small, with elements of the nuclear EFG tensor not exceeding 0.1 au. For both systems, the EFGs becomes less positive/more negative upon picture-change correction, a trend that is also consistently found for the other systems studied in this work. For free uranyl, SO effects on the EFG are moderately strong both before and after correcting for picture-change errors. In the carbonate complex, the SO effects are moderately large for the uncorrected EFGs but small for the picture-change corrected results. The influence from using a model potential to include two-electron spin−orbit corrections in a mean-field sense is noticeable, rendering the EFGs less positive by a few tenth of an atomic unit. However, this correction is small compared to the variations of the EFGs of these systems with different density functionals.[50] For the carbonate complex the picture-change corrections are of the same magnitude as the total EFG. Sizable differences of 1 au between the picture-change corrections obtained from SO versus scalar X2C calculations for this complex show that, for uranium at least, an estimate of the picture-change at a scalar level of theory would not be accurate.

The comparison between the calculated results demonstrates the aforementioned sensitivity to the functional, similar to what has been found previously for some transition metal EFGs.[50,79,89] For the carbonate complex, we obtain almost double the CAM-B3LYP value with HF, and the uranyl values are positive. The increase in the EFG magnitude of the carbonate complex when going from B3LYP to CAM-B3LYP in the X2C calculations is comparable to what has been obtained previously with ZORA-4[50] (ZORA-4: 7.36 to 9.02 au). On the basis of the previous study, nonhybrid DFT field gradients for the carbonate complex are expected to be about 2 au smaller in magnitude than the B3LYP values. Unfortunately, we had difficulties converging such a calculation with X2C despite repeated attempts. The EFGs for free uranyl are consistent with the trends for the carbonate complex: pure DFT gives the least positive, and HF gives the most positive EFG at uranium. For free uranyl the change from DFT to HF is large enough that the EFG at uranium in the HF calculation ends up being positive. It would appear worthwhile to determine the extent of the DFT delocalization error in the different calculations, as done recently for Cu(I) and Au(I) halide diatomics where the EFG at the metal is also very sensitive to approximations in the functional and sign changes between DFT and HF occur.[50,79,89,90] The present CAM-B3LYP result for the carbonate complex agrees quite well with the aforementioned experimental estimate for a structurally closely related nitrate complex, +8.38 ± 0.13 au.[80] To our knowledge, experimental EFGs have not yet been determined for carbonate complexes.

Table 6 lists for UO_2^{2+} the convergence of DKH calculations for increasing order of the decoupling transformation (up to order 35) and the corresponding BSS data. When considering variations of the EFG for different functionals, for instance, the result is already quite accurate at the DKH2 level. For increasing order, an oscillatory convergence toward the BSS value is observed. Both the BSS and DKH35 values differ from the X2C result by 0.01 au. However, we note that this is a very small difference compared to the discrepancy induced by different model potentials, density functionals, or the truncation of the AO basis.

Table 6. Electric Field Gradient (V_{33}, in au) at Uranium in Uranyl[a]

	UO_2^{2+}	
V_{33} (au)	no pcc	w/pcc
DKH2	−5.096	−8.646
DKH3	−5.193	−8.720
DKH4	−5.175	−8.668
DKH5	−5.182	−8.674
DKH6	−5.179	−8.689
DKH7	−5.180	−8.690
DKH8	−5.180	−8.685
DKH35	−5.180	−8.688
BSS	−5.170	−8.687
X2C	−5.304	−8.697

[a]B3LYP functional. Spin−orbit calculations using V_{ext} for the operator transformations.

5. SUMMARY

We have presented relativistic calculations of EFGs in molecules, based on relativistic two-component exact-decoupling approaches that have been implemented in the open-source quantum chemistry package NWChem. Spin−orbit coupling has been included variationally in the ground state calculations. The EFGs at heavy nuclei such as I, At, or U are strongly influenced by picture-change corrections (pcc). Compared to the pcc, the effects from spin−orbit coupling on the EFGs was found to be modest (with the exception of the iodine EFG in TlI) but should not be excluded for accurate predictions. For the At EFG in HAt and the uranium carbonate complex, SO effects on the EFGs were larger before than after picture-change corrections were applied. It remains to be seen whether this is a general trend. Possibly, this finding is a simple consequence of the investigated picture-change corrected EFGs being smaller in magnitude than the uncorrected EFGs for these systems. The calculations on iodine EFGs in group-13 iodide diatomics have shown that the pcc are to some degree transferable between systems and only slightly affected by SO effects. However, for the U EFG in the uranyl-carbonate complex, SO effects on the picture-change correction were seen to reach 1 atomic unit in magnitude. It is therefore recommended that EFG calculations for heavy atoms are carried out with SO coupling and pcc simultaneously. Overall, the calculations demonstrate that exact decoupling methods for two-component DFT calculations are feasible not only for small benchmark systems but also for moderately sized complexes with very heavy elements. A present bottleneck is the memory required to store the matrices entering the decoupling procedure, and potentially the diagonalization step (eq 5). Local decoupling schemes such as those recently proposed by some of us[57] and Seino et al.[93] are expected to eliminate such bottlenecks.

AUTHOR INFORMATION

Corresponding Author

*E-mail: jochena@buffalo.edu.

Notes

The authors declare no competing financial interest.

■ ACKNOWLEDGMENTS

This work has been supported by the US Department of Energy, Basic Energy Sciences, Heavy Element Chemistry program under Grant No. DE-FG02-09ER16066 (grant to J.A.). We thank the Center for Computational Research (CCR) at the University at Buffalo for continuing support of our research projects. J.A. thanks Drs. W. A. de Jong and N. Govind (Pacific Northwest National Laboratory) for technical information related to the NWChem code. D.P. and M.R. acknowledge financial support from the Swiss National Science Foundation SNF.

■ REFERENCES

(1) Dyall, K. G.; Faegri, Jr., K. *Relativistic Quantum Chemistry*; Oxford University Press: New York, 2007.
(2) Reiher, M.; Wolf, A. *Relativistic Quantum Chemistry. The Fundamental Theory of Molecular Science*; Wiley-VCH: Weinheim, Germany, 2009.
(3) Liu, W. *Mol. Phys.* **2010**, *108*, 1679−1706.
(4) Saue, T. *ChemPhysChem* **2011**, *12*, 3077−3094.
(5) Autschbach, J. *J. Chem. Phys.* **2012**, *136*, 150902.
(6) Pernpointner, M.; Visscher, L. *J. Chem. Phys.* **2001**, *114*, 10389−10396.
(7) Autschbach, J.; Zheng, S.; Schurko, R. W. *Concepts Magn. Reson., Part A* **2010**, *36A*, 84−126.
(8) Lucken, E. A. C. *Nuclear Quadrupole Coupling Constants*; Academic Press: New York, 1969.
(9) Dillon, K. B. Nuclear quadrupole resonance spectroscopy. In *Spectroscopic Properties of Inorganic and Organometallic Compounds*; The Royal Society of Chemistry: London, 2005; Vol. *37*, pp 1−15.
(10) Schwerdtfeger, P.; Söhnel, T.; Pernpointner, M.; Laerdahl, J. K.; Wagner, F. E. *J. Chem. Phys.* **2001**, *115*, 5913−5924.
(11) Barone, G.; Mastalerz, G.; Reiher, M.; Lindh, R. *J. Phys. Chem. A* **2008**, *112*, 1666−1672.
(12) Kowalewski, J.; Mäler, L. *Nuclear Spin Relaxation in Liquids: Theory, Experiments, and Applications*; Taylor & Francis: New York, 2006.
(13) Bryce, D. L.; Eichele, K.; Wasylishen, R. E. *Inorg. Chem.* **2003**, *42*, 5085−5096.
(14) Wong, A.; Pike, K. J.; Jenkins, R.; Clarkson, G. J.; Anupold, T.; Howes, A. P.; Crout, D. H. G.; Samoson, A.; Dupree, R.; Smith, M. E. *J. Phys. Chem. A* **2006**, *110*, 1824−1835.
(15) Bryce, D. L.; Sward, G. D. *Magn. Reson. Chem.* **2006**, *44*, 409−450.
(16) Visscher, L.; Enevoldsen, T.; Saue, T.; Oddershede, J. *J. Chem. Phys.* **1998**, *109*, 9677−9684.
(17) Dyall, K. G. *J. Chem. Phys.* **1997**, *106*, 9618−9626.
(18) Dyall, K. G. *J. Chem. Phys.* **1998**, *109*, 4201−4208.
(19) Dyall, K. G.; Enevoldsen, T. *J. Chem. Phys.* **1999**, *111*, 10000−10007.
(20) Dyall, K. G. *J. Chem. Phys.* **2001**, *115*, 9136−9143.
(21) Dyall, K. G. *J. Comput. Chem.* **2002**, *23*, 786−793.
(22) Filatov, M.; Cremer, D. *J. Chem. Phys.* **2003**, *119*, 11526−11540.
(23) Filatov, M.; Cremer, D. *J. Chem. Phys.* **2005**, *122*, 064104.
(24) Jensen, H. J. A. Douglas-Kroll the easy way. Conference on Relativistic Effects in Heavy Elements—Computational Approaches to Spin-Magnetic Properties of Molecules. REHE 2005 Conference, Mülheim, Germany, April, 2005.
(25) Kutzelnigg, W.; Liu, W. *J. Chem. Phys.* **2005**, *123*, 241102.
(26) Kutzelnigg, W.; Liu, W. *Mol. Phys.* **2006**, *104*, 2225−2240.
(27) Liu, W.; Peng, D. *J. Chem. Phys.* **2006**, *125*, 044102.
(28) Filatov, M.; Dyall, K. G. *Theor. Chem. Acc.* **2007**, *117*, 333−338.
(29) Liu, W.; Kutzelnigg, W. *J. Chem. Phys.* **2007**, *126*, 114107.
(30) Iliaš, M.; Saue, T. *J. Chem. Phys.* **2007**, *126*, 064102.
(31) Peng, D.; Liu, W.; Xiao, Y.; Cheng, L. *J. Chem. Phys.* **2007**, *127*, 104106.
(32) Liu, W.; Peng, D. *J. Chem. Phys.* **2009**, *131*, 031104.
(33) Sikkema, J.; Visscher, L.; Saue, T.; Iliaš, M. *J. Chem. Phys.* **2009**, *131*, 124116.
(34) Filatov, M. *J. Chem. Phys.* **2006**, *125*, 107101.
(35) Barysz, M.; Sadlej, A. J.; Snijders, J. G. *Int. J. Quantum Chem.* **1997**, *65*, 225−239.
(36) Barysz, M.; Sadlej, A. J. *J. Mol. Struct. (THEOCHEM)* **2001**, *573*, 181−200.
(37) Barysz, M.; Sadlej, A. J. *J. Chem. Phys.* **2002**, *116*, 2696−2704.
(38) Kędziera, D.; Barysz, M. *Chem. Phys. Lett.* **2007**, *446*, 176−181.
(39) Reiher, M.; Wolf, A. *J. Chem. Phys.* **2004**, *121*, 2037−2047.
(40) Reiher, M.; Wolf, A. *J. Chem. Phys.* **2004**, *121*, 10945−10956.
(41) Wolf, A.; Reiher, M. *J. Chem. Phys.* **2006**, *124*, 064102.
(42) Wolf, A.; Reiher, M. *J. Chem. Phys.* **2006**, *124*, 064103.
(43) Mastalerz, R.; Barone, G.; Lindh, R.; Reiher, M. *J. Chem. Phys.* **2007**, *127*, 074105.
(44) Peng, D.; Hirao, K. *J. Chem. Phys.* **2009**, *130*, 044102.
(45) Kellö, V.; Sadlej, A. J. *Int. J. Quantum Chem.* **1998**, *68*, 159−174.
(46) Baerends, E. J.; Schwarz, W. H. E.; Schwerdtfeger, P.; Snijders, J. G. *J. Phys. B* **1990**, *23*, 3225−3240.
(47) Autschbach, J.; Schwarz, W. H. E. *Theor. Chem. Acc.* **2000**, *104*, 82−88.
(48) Pernpointner, M.; Schwerdtfeger, P.; Hess, B. A. *Int. J. Quantum Chem.* **2000**, *76*, 371−384.
(49) van Lenthe, E.; Baerends, E. J. *J. Chem. Phys.* **2000**, *112*, 8279−8292.
(50) Aquino, F.; Govind, N.; Autschbach, J. *J. Chem. Theory Comput.* **2010**, *6*, 2669−2686.
(51) Neese, F.; Wolf, A.; Fleig, T.; Reiher, M.; Hess, B. A. *J. Chem. Phys.* **2005**, *122*, 204107.
(52) Malkin, I.; Malkina, O. L.; Malin, V. G. *Chem. Phys. Lett.* **2002**, *361*, 231−236.
(53) Peng, D.; Reiher, M. *Theor. Chem. Acc.* **2012**, *131*, 1081.
(54) Nichols, P.; Govind, N.; Bylaska, E. J.; de Jong, W. A. *J. Chem. Theo. Comp.* **2009**, *5*, 491−499.
(55) Feller, D. *J. Comput. Chem.* **2000**, *17*, 1571−1586.
(56) Schuchardt, K.; Didier, B.; Elsethagen, T.; Sun, L.; Gurumoorthi, V.; Chase, J.; Li, J.; Windus, T. *J. Chem. Inf.* **2007**, *47*, 1045−1052.
(57) Peng, D.; Reiher, M. *J. Chem. Phys.* **2012**, *136*, 244108.
(58) Kutzelnigg, W. *Int. J. Quantum Chem.* **1984**, *25*, 107−129.
(59) Dyall, K. G.; Grant, I. P.; Wilson, S. *J. Phys. B* **1984**, *17*, 493−503.
(60) Dyall, K. G. *J. Chem. Phys.* **1994**, *100*, 2118−2127.
(61) Kutzelnigg, W. *Chem. Phys.* **1997**, *225*, 203−222.
(62) Bylaska, E. J.; de Jong, W. A.; Govind, N.; Kowalski, K.; Straatsma, T. P.; Valiev, M.; van Dam, J. J.; Wang, D.; Apra, E.; Windus, T. L.; Hammond, J.; Autschbach, J.; Aquino, F.; Nichols, P.; Hirata, S.; Hackler, M. T.; Zhao, Y.; Fan, P.-D.; Harrison, R. J.; Dupuis, M.; Smith, D. M. A.; Glaesemann, K.; Nieplocha, J.; Tipparaju, V.; Krishnan, M.; Vazquez-Mayagoitia, A.; Jensen, L.; Swart, M.; Wu, Q.; Van Voorhis, T.; Auer, A. A.; Nooijen, M.; Crosby, L. D.; Brown, E.; Cisneros, G.; Fann, G. I.; Fruchtl, H.; Garza, J.; Hirao, K.; Kendall, R.; Nichols, J. A.; Tsemekhman, K.; Wolinski, K.; Anchell, J.; Bernholdt, D.; Borowski, P.; Clark, T.; Clerc, D.; Dachsel, H.; Deegan, M.; Dyall, K.; Elwood, D.; Glendening, E.; Gutowski, M.; Hess, A.; Jaffe, J.; Johnson, B.; Ju, J.; Kobayashi, R.; Kutteh, R.; Lin, Z.; Littlefield, R.; Long, X.; Meng, B.; Nakajima, T.; Niu, S.; Pollack, L.; Rosing, M.; Sandrone, G.; Stave, M.; Taylor, H.; Thomas, G.; van Lenthe, J.; Wong, A.; Zhang, Z. *NWChem, A Computational Chemistry Package for Parallel Computers*, version 6 (2012 developer's version); Pacific Northwest National Laboratory: Richland, WA, 2011.
(63) Kendall, R. A.; Aprà, E.; Bernholdt, D. E.; Bylaska, E. J.; Dupuis, M.; Fann, G. I.; Harrison, R. J.; Ju, J.; Nichols, J. A.; Nieplocha, J.; Straatsma, T. P.; Windus, T. L.; Wong, A. T. *Comput. Phys. Commun.* **2000**, *128*, 260−283.
(64) Valiev, M.; Bylaska, E. J.; Govind, N.; Kowalski, K.; Straatsma, T. P.; Dam, H. J. J. V.; Wang, D.; Nieplocha, J.; Apra, E.; Windus, T. L.; de Jong, W. A. *Comput. Phys. Commun.* **2010**, *181*, 1477.

(65) Tsuchiya, T.; Abe, M.; Nakajima, T.; Hirao, K. *J. Chem. Phys.* **2001**, *115*, 4463−4472.
(66) Weigend, F.; Ahlrichs, R. *Phys. Chem. Chem. Phys.* **2005**, *7*, 3295−3305.
(67) Roos, B. O.; Lindh, R.; Malmqvist, P.; Veryazov, V.; Widmark, P. *J. Phys. Chem. A* **2005**, *109*, 6575−6579.
(68) Becke, A. D. *Phys. Rev. A* **1988**, *38*, 3098−3100.
(69) Perdew, J. P. *Phys. Rev. B* **1986**, *33*, 8822−8824.
(70) Becke, A. D. *J. Chem. Phys.* **1993**, *98*, 1372−1377.
(71) Lee, C.; Yang, W.; Parr, R. G. *Phys. Rev. B* **1988**, *37*, 785−789.
(72) Stephens, P. J.; Devlin, F. J.; Chabalowski, C. F.; Frisch, M. J. *J. Phys. Chem.* **1994**, *98*, 11623−11627.
(73) Yanai, T.; Tew, D. P.; Handy, N. C. *Chem. Phys. Lett.* **2004**, *393*, 51−57.
(74) van Wüllen, C.; Michauk, C. *J. Chem. Phys.* **2005**, *123*, 204113.
(75) Huber, K.; Herzberg, G. Constants of Diatomic Molecules. In *NIST Chemistry WebBook, NIST Standard Reference Database Number 69*; Mallard, W. G., Linstrom, P. J., Eds.; National Institute of Standards and Technology: Gaithersburg, MD, 2005; data prepared by Gallagher, J. W.; Johnson, R. D., III. URL: http://webbook.nist.gov (accessed 8/12/12).
(76) Lucken, E. A. C. Vibrational dependencies and isotope effects on nuclear quadrupole coupling constants. In *Advances in Nuclear Quadrupole Resonance*; Smith, J. A. S., Ed.; Wiley: New York, 1983, pp 83−124.
(77) Van Stralen, J. N. P.; Visscher, L. *Mol. Phys.* **2003**, *101*, 2115−2124.
(78) Pyykkö, P. *Mol. Phys.* **2008**, *106*, 1965−1974.
(79) Schwerdtfeger, P.; Pernpointner, M.; Nazarewicz, W. Calculation of Nuclear Quadrupole Coupling Constants. In *Calculation of NMR and EPR Parameters. Theory and Applications*; Kaupp, M., Bühl, M., Malkin, V. G., Eds.; Wiley-VCH: Weinheim, Germany, 2004, pp 279−291.
(80) Monard, J. A.; Huray, P. G.; Thomson, J. O. *Phys. Rev. B* **1974**, *9*, 2838−2845.
(81) Schreckenbach, G.; Shamov, G. A. *Acc. Chem. Res.* **2010**, *43*, 19−29.
(82) Cho, H.; de Jong, W. A.; Soderquist, C. Z. *J. Chem. Phys.* **2010**, *132*, 084501.
(83) Pepper, M.; Bursten, B. E. *Chem. Rev. B* **1991**, *91*, 719−741.
(84) Clark, D. L.; Hobart, D. E.; Neu, M. P. *Chem. Rev.* **1995**, *95*, 25−48.
(85) Belanzoni, P.; Baerends, E.; van Lenthe, E. *Mol. Phys.* **2005**, *103*, 775−787.
(86) de Jong, W. A.; Visscher, L.; Nieuwpoort, W. C. *J. Mol. Struct. (THEOCHEM)* **1998**, *458*, 41−52.
(87) Schwerdtfeger, P.; Pernpointner, M.; Laerdahl, J. K. *J. Chem. Phys.* **1999**, *111*, 3357−3364.
(88) Bast, R.; Schwerdtfeger, P. *J. Chem. Phys.* **2003**, *119*, 5988−5994.
(89) Thierfelder, C.; Schwerdtfeger, P.; Saue, T. *Phys. Rev. A* **2007**, *76*, 034502−4.
(90) Srebro, M.; Autschbach, J. *J. Phys. Chem. Lett.* **2012**, *3*, 576−581.
(91) Larsson, S.; Pyykkö, P. *Chem. Phys.* **1986**, *101*, 355−369.
(92) Pyykkö, P.; Seth, M. *Theor. Chem. Acc.* **1997**, *96*, 92−104.
(93) Seino, J.; Nakai, H. *J. Chem. Phys.* **2012**, *136*, 244102.